ELSEVIER

Ocean Modelling 4 (2002) 249–267

Ocean Modelling

www.elsevier.com/locate/omodol

Developments in terrain-following ocean models: intercomparisons of numerical aspects

Tal Ezer [a,*], Hernan Arango [b], Alexander F. Shchepetkin [c]

[a] *Program in Atmospheric and Oceanic Sciences, Princeton University, P.O. Box CN710, Sayre Hall, Princeton, NJ 08544-0710, USA*

[b] *Institute of Marine and Coastal Sciences, Rutgers University, 71 Dudley Road, New Brunswick, NJ 08901, USA*

[c] *Institute of Geophysics and Planetary Physics, University of California at Los Angeles, 405 Hilgard Avenue, Los Angeles, CA 90024-1567, USA*

Abstract

During the course of developing new numerical algorithms for a terrain-following ocean modeling system (TOMS), different numerical aspects have been evaluated through a comparison between two widely used community ocean models, the Princeton ocean model (POM) and the regional ocean modeling system (ROMS). While both models aim at modeling coastal to basin-scale problems using similar grids, their numerical algorithms, code structure, and parameterization options are very different. Sensitivity studies with an idealized channel flow and a steep seamount configuration demonstrate how different algorithms in the two models may affect numerical errors, the stability of the code and the computational efficiency. For example, new pressure gradient schemes using polynomial fits and new time stepping algorithms may reduce numerical errors and allow using longer time steps than standard schemes do. However, the new schemes may require more careful choices of time steps and the use of higher order advection schemes to maintain numerical stability.

Keywords: Ocean modeling; Numerical methods; Sigma coordinates

1. Introduction

Free surface, terrain-following (sigma or s-coordinates) ocean models emerged some 20 years ago from the need to model turbulent processes (Mellor and Yamada, 1982) in surface and bottom boundary layers and to simulate flows in estuaries and coastal regions. These efforts led to the development of the Blumberg–Mellor model (Blumberg and Mellor, 1983, 1987) that later became

* Corresponding author. Tel.: +1-609-258-1318; fax: +1-609-258-2850.
E-mail address: ezer@splash.princeton.edu (T. Ezer).

1463-5003/02/$ - see front matter
PII: S1463-5003(02)00003-3

known as the Princeton ocean model (POM). Developments of other ocean models of this class followed with the development of the semi-spectral primitive equation model (SPEM, Haidvogel et al., 1991), the s-coordinate Rutgers model (SCRUM, Song and Haidvogel, 1994), and the regional ocean modeling systems (ROMS, Haidvogel et al., 2000; Shchepetkin and McWilliams, 2000). Earlier versions of the latter models with either vertical spectral schemes or with rigid lid surfaces were replaced by finite three-dimensional differencing and free surface schemes, so that SCRUM and ROMS eventually became very similar to the POM in most aspects. These models use curvilinear orthogonal horizontal coordinates, a horizontal numerical staggered "C" grid (Arakawa and Lamb, 1977), and a vertical staggered grid with either a sigma or a more general s-coordinate system. However, there are considerable differences in numerics and parameterizations between the different models, as will be discussed later. The above models are now in use by over 1000 users world wide. Support to these community models is provided through web and internet communication by Princeton University (http://www.aos.princeton.edu/WWWPUBLIC/htdocs.pom) and Rutgers University (http://marine.rutgers/edu/po). Another sub-class of coastal ocean models which involved finite element (Lynch and Gray, 1980) or spectral element (Iskandarani et al., 1995) methods will not be discussed here; for a more complete review of coastal ocean models see Greatbatch and Mellor (1999) and Haidvogel and Beckmann (1999).

The attractiveness of terrain-following ocean models is in their smooth representation of topography and their ability to simulate interactions between flows and topography. In contrast, z-level models have difficulties in simulating overflow processes and bottom boundary layer dynamics because of the step-like representation of topography (Gerdes, 1993; Beckmann and Döscher, 1997; Winton et al., 1998; Pacanowski and Gnanadesikan, 1998). On the other hand, the numerical error in the pressure gradient calculation over steep topography has been an area of concern for terrain-following ocean models (Haney, 1991; Beckmann and Haidvogel, 1993; Mellor et al., 1994, 1998). While this numerical error can not be completely eliminated as long as the grid does not follow geopotential or isopycnal surfaces, new methods that involve for example, high order or z-level interpolation schemes (McCalpin, 1994; Chu and Fan, 1997, 1998; Kliem and Pietrzak, 1999), or parabolic reconstruction schemes (Shchepetkin and McWilliams, 2002) may reduce this error to an acceptable level below other numerical errors. Some of these pressure gradient methods will be tested here, as well as new time stepping algorithms. While traditionally, terrain-following ocean models were used in the past mostly for regional coastal simulations, there are now a growing number of applications of these models for basin scale (Haidvogel et al., 2000; Ezer and Mellor, 1997, 2000) and even long-term climate studies (Ezer, 1999, 2001). Since large-scale and long-term problems may not allow the use of very high resolution grids, the pressure gradient error in those models may be a larger problem than it is in regional models with finer grids.

The main aim of this paper is to review and evaluate some new developments in terrain-following ocean models. A future expert terrain-following ocean modeling system (TOMS) is now under development and being tested at several institutions. The study follows a recent review of ocean climate models by Griffies et al. (2000) which puts more emphasis on z-level and isopycnal models rather than on sigma-coordinate models. To demonstrate the effect of various numerical schemes and parameterizations, sensitivity experiments and comparisons of two of the most widely used community ocean models, POM and ROMS, are performed. While both models solve the same primitive equations on similar numerical grids, the numerical algorithms, code structure

and modeling concepts in these models are completely different. The basic POM is a simple stand-alone code with limited number of options and standard numerical schemes (e.g., a three-level leap-frog time stepping); the numerical code in the basic POM model structure has not changed much since it was originally developed. New or improved versions such as a non-Boussinesq version (Mellor and Ezer, 1995), a version with a generalized coordinate system (Mellor et al., 2002) or high order pressure gradient schemes (Chu and Fan, 1998) are provided as stand-alone codes or replacement subroutines. Because of its simplicity and robustness POM quickly became very popular (during the last decade the number of POM users roughly doubles every two years); the model is especially popular in many countries and institutions with limited computational resources. The concept of ROMS (and TOMS) on the other hand is to provide the best and newest available algorithms in a modular code similar to the concept of the modular ocean model (MOM, Pacanowski and Griffies, 1999). A large number of choices, including different advection, diffusion and pressure gradient schemes, different boundary conditions, and even data assimilation schemes can be selected; the desired executable code is configured through a C-language pre-processing (CPP) commands. The variety of options in ROMS provides users with a larger flexibility than that provided to POM users, but users may need more knowledge on the behavior of the model under different parameterizations and a longer learning period than that of a simpler code. Because of these differences, the ROMS code is almost 20 times larger than the POM code; however, some of its advanced numerics may be more accurate and relatively more efficient than standard codes are, as will be shown below.

2. The seamount test case configuration

A channel flow over and around a tall seamount (on an *f*-plane) is an idealized, but difficult to resolve problem, that is implemented for this study. The studies of Beckmann and Haidvogel (1993) and Mellor et al. (1998) have used a similar configuration. The topography includes a square domain with closed boundaries in the north and south and a steep seamount in the center of the domain (Fig. 1). The bottom topography is defined by

$$H(x,y) = H_{\max}[1 - A\,\mathrm{e}^{-(x^2+y^2)/L^2}]. \tag{1}$$

The maximum depth is $H_{\max} = 4500$ m in all the cases. Two experimental designs, a "very steep" case with $A = 0.9$ and $L = 25$ km and a "moderately steep" case with $A = 0.6$ and $L = 50$ km are used. The initial temperature (in °C) depends only on $-H_{\max} < z < 0$, and defined by

$$T(x,y,z) = 5 + 15\,\mathrm{e}^{z/1000}. \tag{2}$$

Salinity is constant at 35 psu (a similar, non-linear equation of state is used by both models). A constant eastward flow of 0.2 m s^{-1} is imposed on the east and west open boundaries, which results in about 1 m surface elevation change across the 512 km wide channel. (An exception is the pressure gradient test of Section 3.3, where closed boundary conditions with no external forcing replaces the channel flow.) The horizontal model grid includes 64×64 grid cells with a constant grid size of $\Delta x = \Delta y = 8$ km. With this resolution, the maximum slope parameter $s = |\Delta H|/2H$ (Beckmann and Haidvogel, 1993; Mellor et al., 1998) and the maximum so-called "hydrostatic consistency" parameter $r = |\sigma \Delta H/H\Delta\sigma|$ (Haney, 1991) are $s = 0.07$ and $r = 2.7$ for the

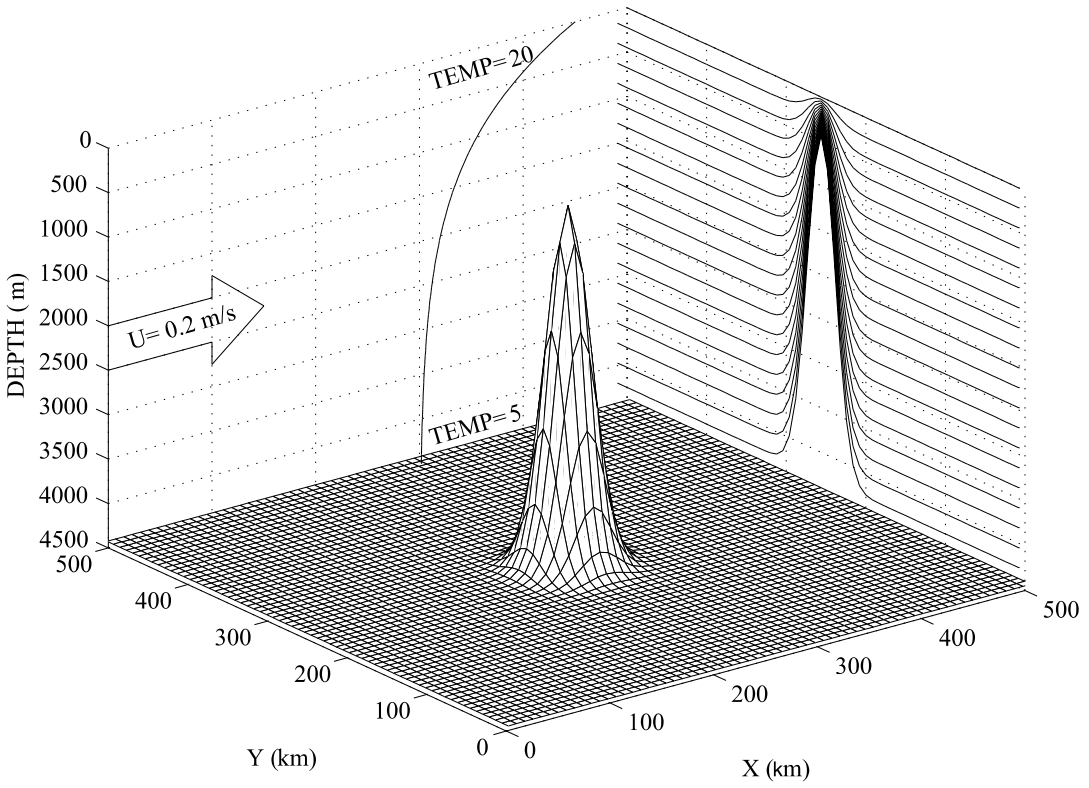

Fig. 1. A diagram of the seamount setup configuration (the very steep case). The temperature profile is shown on the north wall of the domain and the sigma layers are shown on the eastern boundary of the domain.

moderately steep case (similar to Shchepetkin and McWilliams (2002)) and $s = 0.36$ and $r = 14.2$ for the very steep case (similar to Beckmann and Haidvogel (1993), and Mellor et al. (1998)). The vertical grid includes 20 active "standard" sigma layers evenly distributed such that $\sigma = (z - \eta)/(H + \eta)$, where η is the free surface and $-1 < \sigma < 0$ (the more general s-coordinate system in ROMS was set to match the standard POM distribution of layers and we adopt the POM formalism here). It should be mentioned that, both, POM and ROMS, allow variable horizontal grids (e.g., an increase resolution over the seamount as in Mellor et al. (1998)), or uneven and more general vertical layer distributions, not necessarily conforming to the standard sigma (e.g., increase resolution near the surface or bottom such as in Song and Haidvogel (1994) and in Mellor et al. (2002)). However, for simplicity and ease of the comparison, these options have not been used here. To allow a fair comparison between the models, no attempt is made to optimize the vertical grid spacing for each model.

3. Results and comparisons

In the following sections we examine some of the numerical aspects and differences between the two models. For a complete detailed description of the models' equations the reader is referred to

other sources (Blumberg and Mellor, 1987; Mellor, 1996; Haidvogel et al., 2000; Shchepetkin and McWilliams, 2000, 2002); here we only highlight some important differences in numerical algorithms and demonstrate how these differences may affect the results and the choices of parameters.

3.1. Subgrid-scale parameterizations and advection schemes

Both models provide a variety of horizontal and vertical advection and diffusion parameterizations and options; many more options are available in the modular ROMS compared to a limited number of options in POM. For the vertical mixing, both models provide the Mellor–Yamada (MY) level 2.5 closure scheme (Mellor and Yamada, 1982), POM includes also a recently improved version of the MY scheme (Ezer, 2000; Mellor, 2001). ROMS provides additional options for Brunt–Vaisala dependent mixing and a non-local K-profile parameterization (KPP) (Large et al., 1994). The often used choices are MY for POM and KPP for ROMS. For horizontal mixing of tracers the standard POM code provides only a Laplacian, along-sigma, velocity-dependent Smagorinsky diffusivity (Ezer and Mellor, 2000; Mellor and Blumberg, 1985; Smagorinsky, 1963). ROMS provides additional options, including the Gent–McWilliams eddy induced mixing (Gent and McWilliams, 1990). Horizontal mixing of tracers and momentum in ROMS can be rotated to be along sigma (or s) surfaces, along geopotential (z) or along isopycnals (ρ), and there is a choice of constant Laplacian or Biharmonic formulation. Discussion of the advantages and disadvantages of the above schemes are beyond the scope of this paper (but see for example the review by Griffies et al. (2000)).

Advection is of major importance for coastal ocean models if processes such as sediment transport or estuarine and river outflows are to be modeled, as well as for climate studies where deep water formation and eddy driven transports may be important. Since the simple and commonly used second order centered differencing advection scheme may produce an artificial "overshoot" of tracer values for sharp fronts, many alternative advection schemes with various levels of complexities have been developed (see for example recent comparisons of different advection schemes by Pietrzak (1998), and by Hecht et al. (2000)). As alternatives to the second order centered advection scheme in the standard POM code, a few well known upstream biased second and third order schemes are now available to users (Lin et al., 1994; Smolarkiewicz, 1984). ROMS, on the other hand, provides a set of newly implemented advection schemes for momentum and tracers (Shchepetkin and McWilliams, 1998, 2000), which include second (CADV2) and fourth (CADV4) order centered horizontal and vertical advection schemes, and third (UADV3) and fourth order upstream biased advection schemes. Table 1 and Fig. 2 summarize the computational cost of some of these schemes when implemented in POM or ROMS (see more on the computational cost in the next section).

To demonstrate the effect of the different advection schemes we compare here three schemes and two models. In this difficult test of forced flow over a very steep seamount, horizontal diffusion is null, but nevertheless both models are numerically stable. Because of the smooth representation of topography in terrain-following ocean models, these models can handle much lower diffusivities than z-level models with a step-like topography, as demonstrated recently by Mellor et al. (2002). The mean properties across the channel, which include a 1 m sea level change and 450 Sv ($1\ \mathrm{Sv} = 10^6\ \mathrm{m^3\ s^{-1}}$) total transport, hardly show any visible differences between the different experiments. Therefore, only the anomalies relative to the zonal means are shown; these are the

Table 1
Comparisons of computational costs for POM and ROMS when using different features

Basic model	Model features[a]	Computation time per grid point per time step (in 10^{-3} s)	Computation time for one day of integration (in s)
POM	CADV2	12.5	21.3
POM	UADV2	13.2	
POM	MPDATA2	14.0	
POM	MPDATA3	17.1	
POM	CCD6	207.4	
POM	ZINT	40.0	
ROMS	CADV2	17.3	21.6
ROMS	CADV4	19.3	
ROMS	UADV3	20.0	

The grid configuration includes $64 \times 64 \times 20$ active grid cells with a resolution of 8 km. All the experiments were done with serial codes running on a Cray T90 super-computer.

[a] CADV2– second order centered advection scheme, UADV2 – second order upstream-biased advection scheme (Lin et al., 1994), MPDATA2 – second order upstream-biased advection scheme (multidimensional positive definite advection transport algorithm based on Smolarkiewicz, 1984), MPDATA3 – third order upstream-biased advection scheme (MPDATA with three iterations), CCD6 – sixth order combined compact difference pressure gradient scheme (Chu and Fan, 1997, 1998), ZINT – *z*-level interpolation pressure gradient scheme (Kliem and Pietrzak, 1999), CADV4 – fourth order centered advection scheme (Shchepetkin and McWilliams, 1998, 2000), UADV3 – third order upstream-biased advection scheme (Shchepetkin and McWilliams, 1998, 2000).

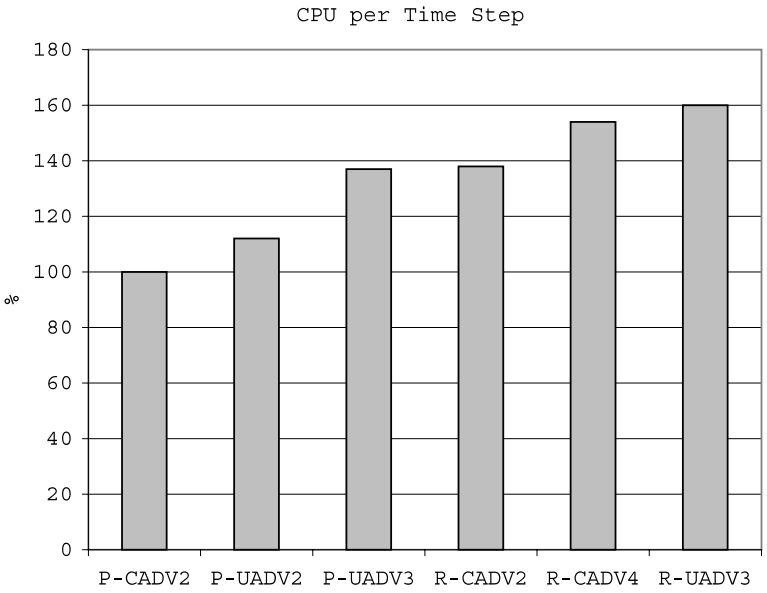

Fig. 2. Computational cost per time step of different codes: standard POM with second order centered advection scheme (P-CADV2), POM with second order upstream-biased advection scheme (P-UADV2), POM with third order upstream-biased advection scheme (P-UADV3), ROMS with second order centered advection scheme (R-CADV2), ROMS with fourth order centered advection scheme (R-CADV4), and ROMS with third order upstream-biased advection scheme (R-UADV3). Values are in percent relative to the standard POM. All calculations refer to serial codes with $64 \times 64 \times 20$ grid points running on one Cray T90 processor and excluding compilation time.

surface elevation (Fig. 3) and the barotropic stream function (Fig. 4) after five days of integration (the minimum, maximum and standard deviation are also indicated in those figures). The modification of the zonal flow by the seamount includes an asymmetric sea level increase upstream the seamount and sea level decrease downstream the seamount (Fig. 3), and the development of cyclonic and anticyclonic circulation cells (Fig. 4). Pressure gradient errors (discussed later) are responsible for changes of the order of a few tenths of cm in sea level anomaly and of the order of 1 Sv in transport, but only affect the area in the very close vicinity of the seamount (here both models use a similar density Jacobian pressure gradient scheme). Most of the differences in the solutions are the result of the advection schemes. When both POM and ROMS use a second order centered advection scheme (top panels of Fig. 3), POM seems to produce a smoother elevation field, a possible result of the smaller numerical diffusion in ROMS. The fourth order centered advection scheme (Fig. 3(d)) is even noisier than the second order scheme for this case, but the third order upstream biased scheme (the default in ROMS, Fig. 3(c)), which has more numerical

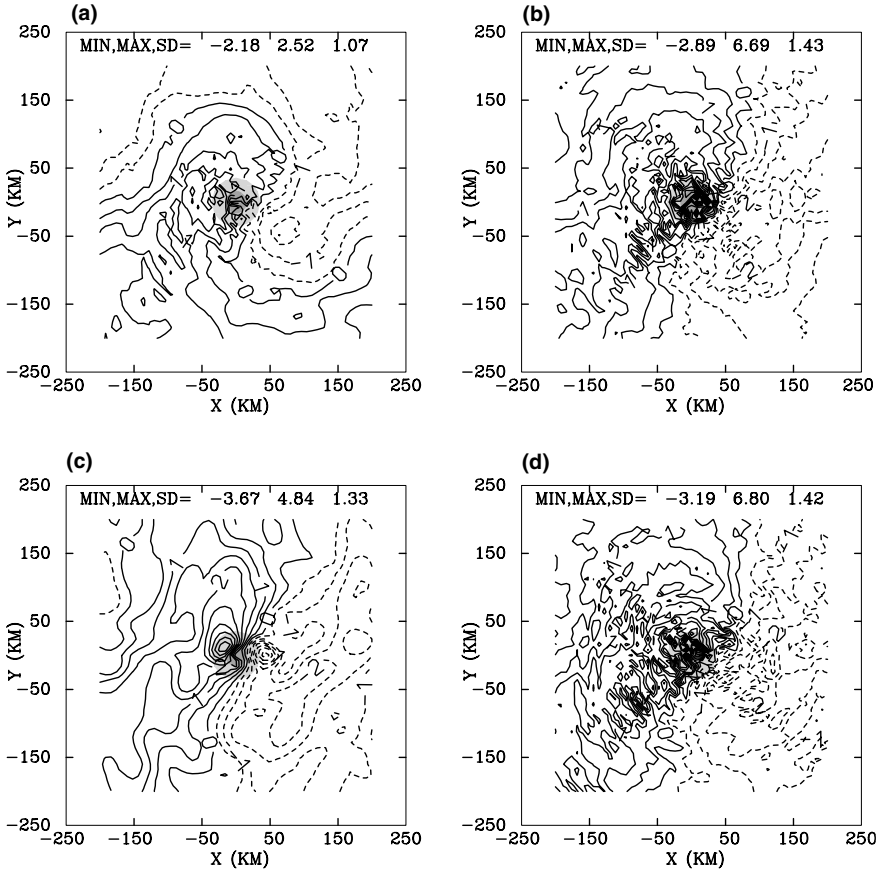

Fig. 3. Surface elevation anomaly (relative to the zonal mean) after five days using different advection schemes: (a) POM with a second order centered scheme, (b) ROMS with a second order centered scheme, (c) ROMS with a third order upstream biased scheme, and (d) ROMS with a fourth order centered scheme. Contour interval is 0.5 cm; minimum, maximum and standard deviation values (in cm) are indicated at the top of each panel.

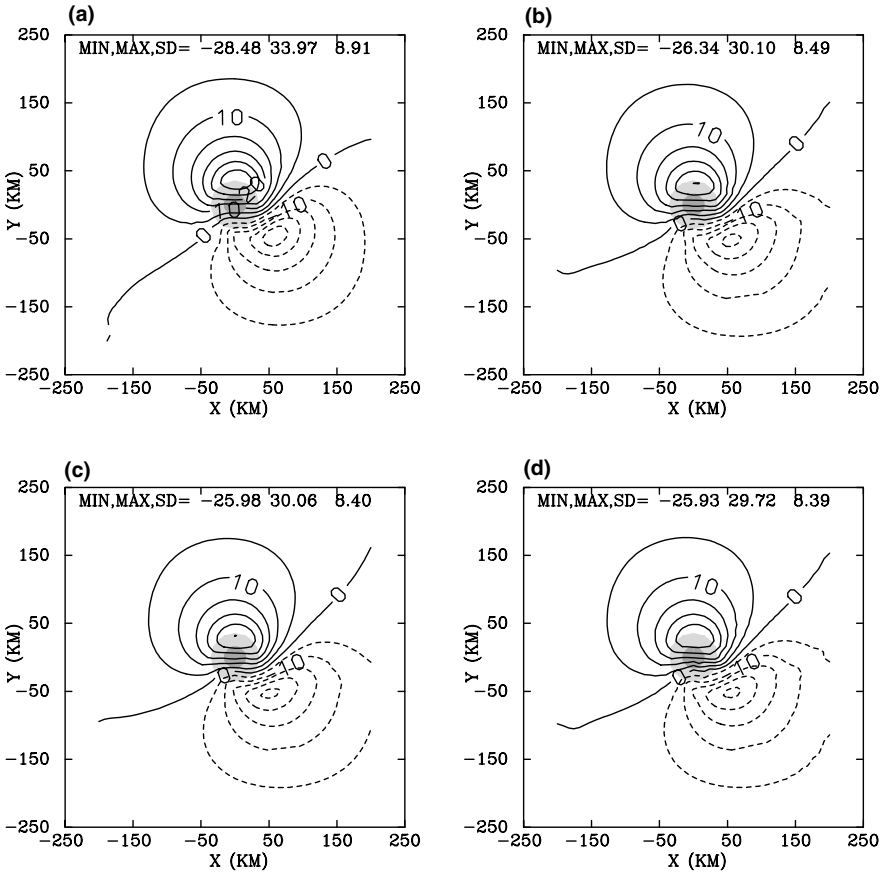

Fig. 4. Same as Fig. 3, but for the stream function anomaly. Contour interval is 5 Sv.

diffusion compared with centered schemes, provides a much smoother solution without the need for additional diffusion. Experiments (not shown) where Laplacian diffusion of 50, 100 and 500 $m^2\ s^{-1}$ were added, show similar smoother solutions using POM for all cases with the centered schemes. The choice of advection scheme has little effect (< 1 Sv) on the model barotropic transport, but there are some differences in transports between the two models due to differences in the numerical advection and in pressure gradient calculations (see Section 3.3).

3.2. Time stepping schemes

Both, POM and ROMS models, use time splitting schemes, where the two-dimensional, vertically integrated momentum equations (i.e., the "external mode") are solved using a short time step to resolve fast moving barotropic waves, and the three-dimensional momentum equations (i.e., the "internal mode"), are solved using a longer time step. This splitting technique is common to many free surface ocean models, since it is more efficient than solving the three-dimensional equations with a short time step required by the Courant–Friedrichs–Lewy (CFL) stability condition (Courant et al., 1967). However, the different truncation errors in the two sets of

equations require numerical adjustments or filters to make sure that the equations correctly satisfy the continuity equations and conserve tracers quantities. POM and ROMS use different time stepping schemes and different filtering technique in their time splitting algorithms, as described below.

The standard POM uses an explicit, second order in time, "leap-frog" (LF) numerical scheme (except the vertical diffusion terms in the internal mode which uses an implicit scheme to allow a high vertical resolution near the surface). Therefore, the time stepping of horizontal advection and horizontal diffusion of a property Q can be written in the general form,

$$Q^{n+1} = Q^{n-1} + 2\Delta t[\mathrm{adv}(Q^n) + \mathrm{dif}(Q^{n-1})], \tag{3}$$

where $n-1, n$ and $n+1$ represent the three time levels, $t-\Delta t$, t, and $t+\Delta t$, respectively, and Δt is the appropriate time step (internal or external). To prevent the well-known time-splitting problem of diverging odd and even time steps associated with the centered time differencing scheme, a simple Asselin filter (Asselin, 1972) is applied at each time step, so the smoothed solution is

$$Q_s^n = Q^n + \alpha/2(Q^{n+1} - 2Q^n + Q_s^{n-1}), \tag{4}$$

where $\alpha = 0.05$ is often used. A simple adjustment of the internal velocities to the vertically integrated external velocities at each *internal* time step is used in POM (in contrast, as explained below, a more sophisticated filter in ROMS couples the two modes every *external* time step). The most restrictive condition for choosing the time step in POM is usually the CFL computational stability condition for the external time step,

$$\Delta t_{\mathrm{E}} \leqslant C^{-1}[(\Delta x)^{-2} + (\Delta y)^{-2}]^{-1/2}, \quad C = 2(gH)^{1/2} + U_{\max}. \tag{5}$$

H is the depth, g is the gravitational acceleration and $U_{\max}$ is the maximum velocity. A similar condition for the internal time step, where C is replaced by the internal gravity wave speed, permits a larger time step than (5). The recommended ratio between the internal and the external time steps, $\Delta t_{\mathrm{I}}/\Delta t_{\mathrm{E}}$, is about 20–80; we will perform later some sensitivity experiments to explore the effect of this ratio on the stability of the two models.

While the above LF numerical time stepping in POM is simple and relatively standard, ROMS uses a predictor-corrector (PC) time stepping which in its general form (some variations for different terms are being tested) involves two steps, a LF predictor step of the form

$$Q^{n+1,*} = Q^{n-1} + 2\Delta t\ \mathrm{func}(Q^n) \tag{6}$$

and a corrector step of the form

$$Q^{n+1} = Q^n + \Delta t\ \mathrm{func}(a_1 Q^{n+1,*} + a_2 Q^n + a_3 Q^{n-1}). \tag{7}$$

The coefficients $(a_1, a_2, a_3) = (5/12, 2/3, -1/12)$ are as in the Adams–Moulton algorithm (Canuto et al., 1988). The additional computational cost of the PC scheme compared with the centered in time scheme may be offset by allowing the use of a larger time step (see Shchepetkin and McWilliams (2000) for detail analysis of the stability properties of the scheme). The coupling of the barotropic (external) and baroclinic (internal) modes in ROMS uses a Gaussian-like filter so that for example the vertically averaged U component of velocity in the baroclinic mode (indicated by a subscript c) is coupled to the barotropic component (indicated by a subscript t) according to

$$\bar{U}_c^{n+1} = \sum_{m=1}^{N} a^m \bar{U}_t^m, \tag{8}$$

where there are N fast barotropic time steps in each baroclinic time step n. The weights a^m are chosen such that the continuity equation is exactly satisfied (Shchepetkin and McWilliams, 2000). Here we will try to demonstrate the sensitivity of the scheme to different time step choices and compared it with the POM scheme for one particular configuration.

A series of sensitivity experiments was performed with both models using identical configuration, a constant horizontal Laplacian viscosity of 500 $m^2\ s^{-1}$ and a constant vertical mixing coefficient of $2 \times 10^{-5}\ m^2\ s^{-1}$. In each experiment the model (either POM or ROMS) was executed for five days with different internal and external time steps, and the solution was checked for its stability by evaluating properties such as surface elevation and kinetic energy, the results are summarized in Table 2. A solution is defined to be unstable if the model blew up or if the variations in total kinetic energy do not decay within the simulated period. As expected, the maximum external time step in POM is determined by the CFL condition (actually allowing a maximum external time step slightly larger than the theoretical one). The regime of stable solutions in ROMS is quite different, allowing the use of internal time steps about 1.5 times larger than in POM and external time step of about twice that allowed by the CFL condition. For short internal time steps POM does seem to be more stable, allowing the use of longer external time step than ROMS does for the same internal time step (e.g., for a baroclinic time step of $\Delta t_I = 180$ s in Table 2, POM requires only 11 barotropic substeps, while ROMS requires 22). Users of these models should be aware of these differences in behavior when choosing the time steps for particular applications. For the same parameterizations (with a centered second order advection scheme) ROMS requires about 40% more computational time per time step than the standard POM does and for the ROMS default of a third order upstream biased advection scheme ROMS requires about 60% more computational time per time step than the standard POM does (Table 1 and Fig. 2). However, when taking into account the maximum time step allowed by the numerical stability of the two models, the computational time required, say, one day of integration, is almost

Table 2
The sensitivity of the model stability to 3D/internal time step (Δt_I in columns) and 2D/external time step (Δt_E in rows)

Model	Δt_E (s)	$\Delta t_I = 180$ s	$\Delta t_I = 360$ s	$\Delta t_I = 540$ s	$t_I = 720$ s	$\Delta t_I = 900$ s	$\Delta t_I = 1080$ s
POM	8	22	45	67	90	Unstable	Unstable
POM	12	15	30	45	60	Unstable	Unstable
POM	16	11	22	34	45	Unstable	Unstable
POM	20	Unstable	Unstable	Unstable	Unstable	Unstable	Unstable
ROMS	8	22	45	67	90	112	Unstable
ROMS	12	Unstable	30	45	60	75	Unstable
ROMS	16	Unstable	22	34	45	56	Unstable
ROMS	20	Unstable	18	27	36	45	Unstable
ROMS	24	Unstable	Unstable	22	30	37	Unstable
ROMS	28	Unstable	Unstable	19	25	32	Unstable
ROMS	32	Unstable	Unstable	Unstable	Unstable	Unstable	Unstable

The values of Δt_E were rounded to the nearest whole numbers. The split mode ratio $\Delta t_I/\Delta t_E$ is indicated for each pair of time steps with a stable solution. The CFL stability condition for an 8 km grid mesh implies $\Delta t_E < 13$ s.

identical in the two models (right column of Table 1) due to the largest time step that can be used in ROMS. One should keep in mind the fact that the number of lines of code in the modular ROMS is about 20 times the number of lines in the simpler POM code (e.g., for this application, compilation time is 70 s for POM and 600 s for ROMS and memory required is 29 Mb for POM and 45 Mb for ROMS); therefore, the ROMS code is quite efficient considering its size. Further comparisons of the performance of the models on massively parallel computers will be reported in a separate paper.

The spinup during the adjustment process is quite different between the two models (Fig. 5), with apparent strong decaying fluctuations in ROMS but not in POM, where the oscillations decay during the first day of integration. The slightly more energetic flow field in ROMS may relate to its small numerical diffusion. While future versions of ROMS may use improved schemes with reduced oscillatory behavior, it is nevertheless important to understand the adjustment process in ROMS. Fig. 6 shows the result of varying the time steps Δt_{I} and Δt_{E} (in the very steep seamount case). The solution converges faster when the external time step decreases (upper panels), but also when the internal time step increases (i.e., when there are more barotropic time steps for each baroclinic time step, right panels). This behavior contradicts the common thinking (and the behavior of POM and other models with standard time stepping algorithms) of increased stability with decreasing time step, but is the result of the predictor–corrector time stepping and in particular, the effect of the filter coupling the two modes. If the ratio between the two modes is

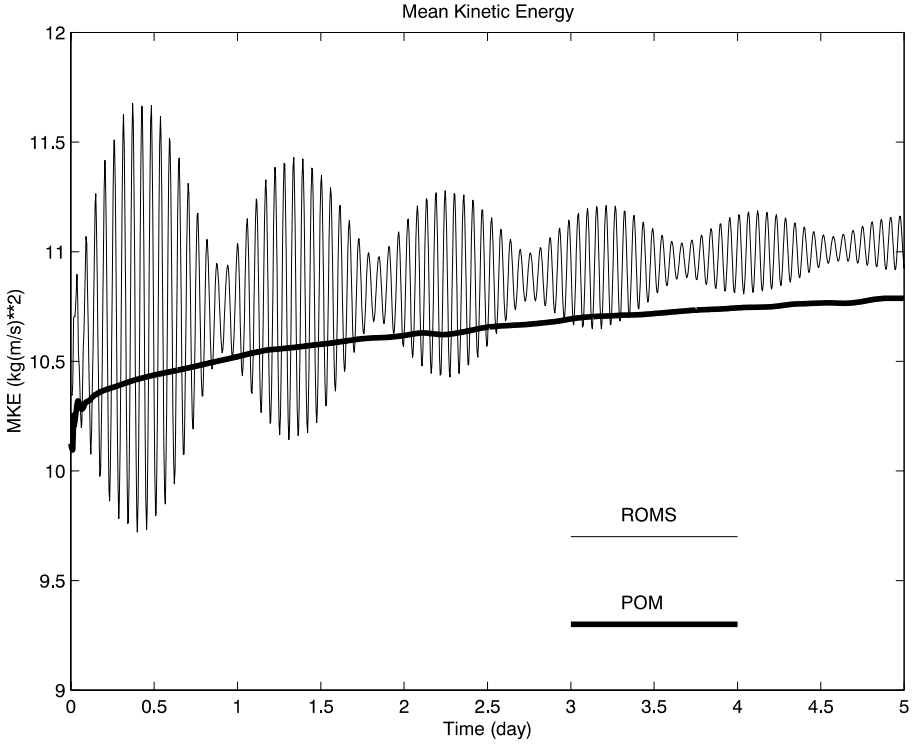

Fig. 5. Variations of mean kinetic energy for a channel flow over a very steep seamount for ROMS (thin line) and POM (heavy line). Both models use the same time steps, $\Delta t_{\mathrm{I}} = 360$ s, $\Delta t_{\mathrm{E}} = 12$ s.

large, a strong coupling is applied by the filter. In ROMS, unlike POM, every fast time step is used in the coupling to the slow time stepping, thus choosing a longer baroclinic time step implies a filter with a wider band and the solution is less prone to numerical instability associated with the splitting modes.

Fig. 7 shows the dependency of the adjustment process to different bottom topographies. For a medium seamount case with less steep slopes (Fig. 7(b)), the kinetic energy increases, probably due to a decrease in the blocking of the mean flow by the Taylor Column effect; additional modulation of the fluctuations are seen as well. Even flat bottom cases (Figs. 7(c) and (d) show similar fluctuations, indicating that the oscillations are not the result of pressure gradient errors over the steep topography (discussed later). The period of the high frequency oscillation is 85 min for the case with a water depth of 4500 m (Fig. 7(c)) and 111 min for the case with a water depth of 2500 m (Fig. 7(d)), exactly the time it takes a barotropic gravity wave to propagate across the channel and back, with a phase propagation speed given by $C = (gH)^{1/2}$. Therefore, these oscillations are clearly related to the adjustment of basin-scale barotropic waves. Experiments with no stratification (not shown) have similar oscillations thus confirming that these are barotropic waves. The Aselin filter in POM (applied only at every baroclinic time step) seems to damp the barotropic waves much faster than the coupling filter in ROMS which is applied at every barotropic time step. The lower frequency modulations, with periods of about one day, do not depend on the time step and are believed to be due to inertial oscillations.

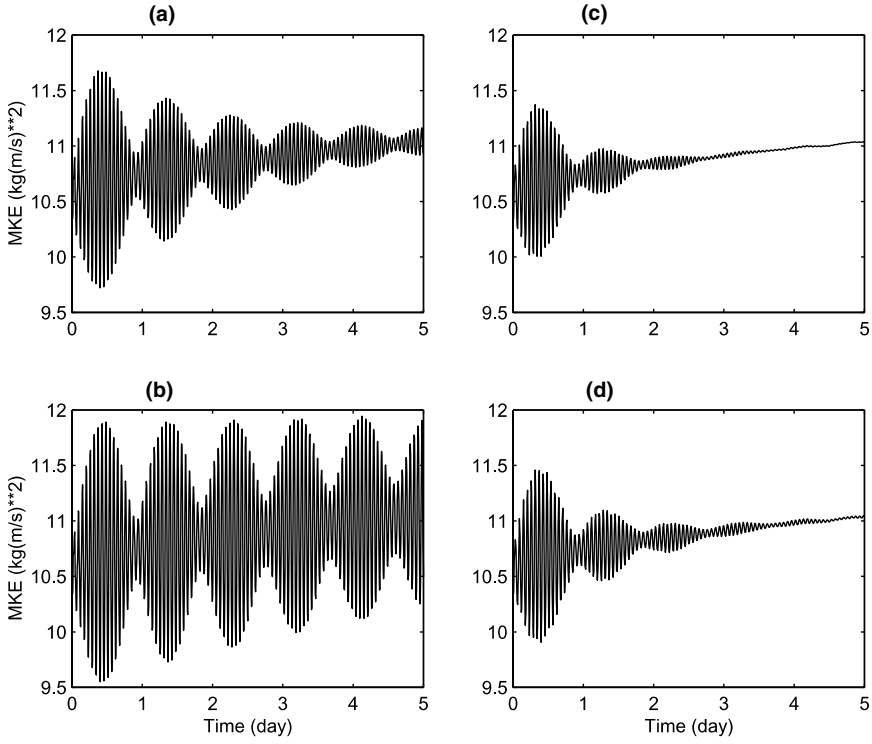

Fig. 6. Variations of mean kinetic energy in ROMS for the steep seamount case with various time steps: (a) $\Delta t_E/\Delta t_I = 12$ s/360 s, (b) $\Delta t_E/\Delta t_I = 24$ s/360 s, (c) $\Delta t_E/\Delta t_I = 12$ s/720 s, and (d) $\Delta t_E/\Delta t_I = 24$ s/720 s.

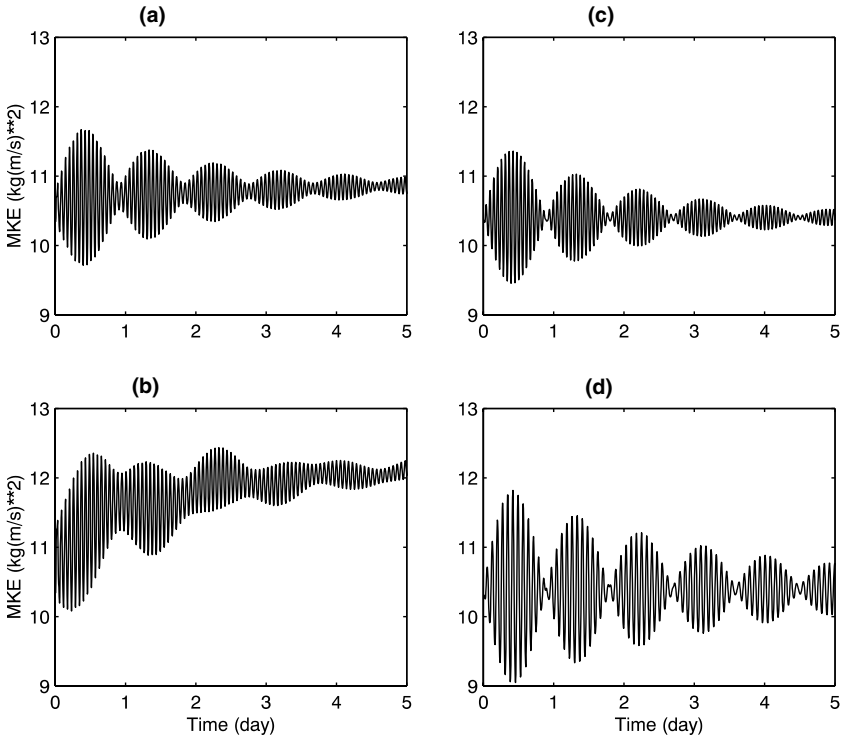

Fig. 7. Same as Fig. 5, but for various bottom topographies: (a) very steep seamount, (b) medium steep seamount, (c) flat bottom with a depth of 4500 m, and (d) flat bottom with a depth of 2500 m.

3.3. Pressure gradient schemes

Pressure gradient errors over steep topography in terrain-following ocean models have been an issue of concern for a long time (Haney, 1991; Beckmann and Haidvogel, 1993; Mellor et al., 1994, 1998). In additional to common remedies such as removing a mean density profile and bottom topography smoothing, several more sophisticated (and often more computationally expensive, Table 1) approaches have been tried in order to reduce such numerical errors to acceptable levels, they include for example high order schemes (McCalpin, 1994; Chu and Fan, 1997, 1998) and interpolation to z-levels (Kliem and Pietrzak, 1999). Recent efficient parabolic spline schemes reconstruct pressure or density fields (Shchepetkin and McWilliams, 2000, 2002); these schemes promise great improvements in accuracy and are compared here against other schemes.

The above seamount test case is now used to study the pressure gradient errors in ROMS and POM. With no external forcing, and initial vertical stratification with no horizontal density gradients according to (2) (and with no removal of a mean density profile; its removal is a common practice in POM), any calculated velocity is considered an error. During a prognostic run the erroneous velocities will create density changes until an adjusted stage is reached through advection and diffusion processes. The seamount case is an especially difficult test since it includes the well known two-dimensional "sigma errors of the first kind", discussed by Haney (1991) and

Mellor et al. (1994), but it is also subject to three-dimensional "sigma errors of the second kind" which depend on the curvature of the topography and produce an eight-lobe error field structure around the seamount (Mellor et al., 1998). Seven pressure gradient algorithms between the two models are evaluated for the same problem configuration:

(1) POM with a standard density Jacobian scheme (Mellor et al., 1998), P-DJ.
(2) POM with a sixth order, combined compact difference scheme (Chu and Fan, 1997), P-CCD.
(3) ROMS with a finite-volume pressure Jacobian scheme (Lin, 1997), R-FPJ.
(4) ROMS with a weighted density Jacobian scheme (Song, 1998), weighting parameter gamma = 0, R-DJ.
(5) ROMS with a weighted density Jacobian scheme (Song, 1998), weighting parameter gamma = 0.125, R-WDJ.
(6) ROMS with a pressure Jacobian scheme using monotonized quadratic polynomial fits (Shchepetkin and McWilliams, 2002), R-PJQ.
(7) ROMS with a density Jacobian scheme using monotonized cubic polynomial fits (Shchepetkin and McWilliams, 2002), R-DJC.

For a complete evaluation of these schemes for various parameters and detailed numerical descriptions one should refer to the appropriate references given above, here we only highlight the basic differences between the schemes and demonstrate how they affect POM and ROMS calculations. The ROMS weighted scheme, R-WDJ, effectively moves the location of the averaged density in a model grid cell depending on the gamma parameter in ROMS. For gamma = 0 (R-DJ) the scheme should be identical to POM's P-DJ scheme, for gamma = 0.25 the scheme should be similar to the original Song (1998) scheme, and gamma = 0.125 was found to be an empirically optimal value (Shchepetkin and McWilliams, 2002, note however a difference in notation with a factor of 4 between the parameter used in the above paper and that used in ROMS and here). The polynomial fit schemes, R-PJQ and R-DJC, reconstruct the pressure or density fields and then use an analytical integration.

The comparison between all pressure gradient algorithms in terms of mean kinetic energy error is shown in Fig. 8 and the maximum velocity errors are summarized in Table 3. One should keep in mind that in these tests (in particular the very steep seamount case) the maximum slopes are larger than in most practical applications and these experiments are intended to test schemes to their extreme limits. The removal of mean density profiles in POM and topographical smoothing to reduce r and s will result in smaller errors than those shown in Table 3. First, we noticed that the finite volume pressure Jacobian scheme of Lin (1997), R-FPJ, did not perform well due to its difficulty in resolving the large curvature of the steep seamount (it blew up in the very steep seamount case, as did the pressure Jacobian scheme, R-SPJ). When ROMS uses a density Jacobian scheme similar to that used in POM, the errors are somewhat larger than in POM due to differences in the stability of the basic numerics. However, the three more elaborated schemes (R-WDJ, R-PJQ, and R-DJC) reduce errors considerably (Fig. 8(a)). The smallest error is obtained in the high order accurate density Jacobian scheme with monotonized cubic polynomial fits (R-DJC) used in ROMS. The small error in R-DJC is comparable to the sixth order scheme (P-CCD) used in POM for the moderate seamount case, but R-DJC is computationally an efficient scheme that does not require more computations than the other schemes, while P-CCD is extremely expensive

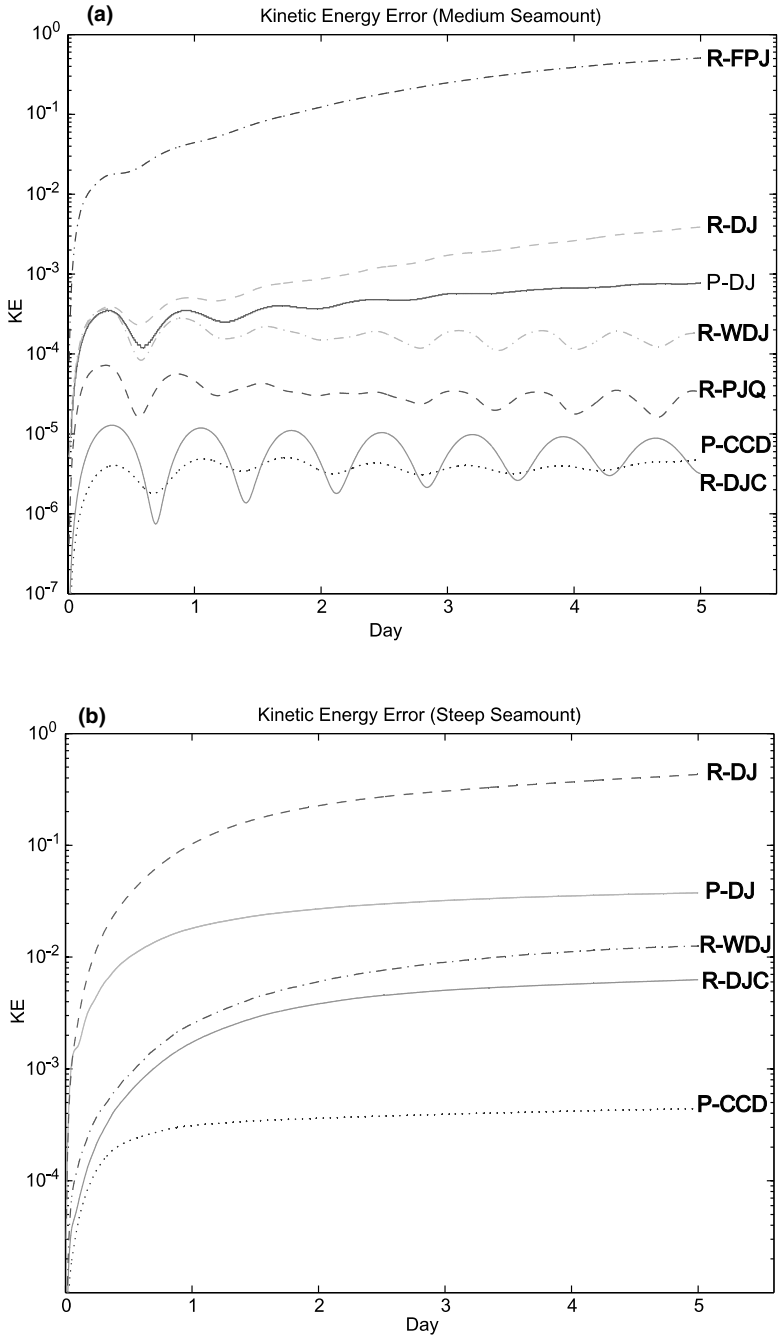

Fig. 8. Mean kinetic energy error (in kg m^2 s^{-2}) for different pressure gradient schemes (see text for notations): (a) the moderately steep and (b) the very steep seamount cases. Schemes that blew up are not shown.

in the way it is currently written (Table 1). In the extremely steep seamount case the high order scheme is the most accurate one, while both R-DJC and the weighted scheme R-WDJ have similar

Table 3
Summary of pressure gradient errors for different schemes

Pressure gradient scheme	Seamount configuration	Maximum barotropic velocity error (cm s^{-1})	Maximum baroclinic velocity error (cm s^{-1})
P-DJ	Very steep	10.9	25.5
	Steep	0.98	1.88
P-CCD	Very steep	1.6	3.1
	Steep	0.02	0.17
R-FPJ	Very steep	*	*
	Steep	30.0	56.0
R-DJ	Very steep	31.7	81.3
	Steep	3.7	5.9
R-WDJ	Very steep	13.4	19.8
	Steep	0.35	0.85
R-PJQ	Very steep	*	*
	Steep	0.03	0.3
R-DJC	Very steep	11.0	14.2
	Steep	0.06	0.13

Cases which blew up before day 5 are marked by "*". Results with relatively small errors (barotropic velocity less than 2 cm s^{-1} and baroclinic velocity less than 4 cm s^{-1}) are underlined. See text for definitions of the schemes.

errors. Polynomial fitting of density rather than pressure seems especially advantageous for a very steep topography. The magnitude of the pressure gradient error depends also on the horizontal and vertical advection of tracers, time-stepping, and the equation of state for seawater (Shchepetkin and McWilliams, 2002), but the relative performance of the various schemes should stand for other parameterizations than those tested here. It should be noted that the relatively short adjustment time obtained here, in Beckmann and Haidvogel (1993), and in Mellor et al. (1998), compared with the much longer time scale in Shchepetkin and McWilliams (2002) relate to the much lower diffusion used in the latter study.

4. Discussion and conclusions

The paper reviewed some of the new developments in ocean models that will lead to a new modular, expert, terrain-following ocean modeling system (TOMS) now under development and testing at several institutions. Modular configuration provides users with many parameterizations and numerical options, but also requires considerable testing to provide users with enough knowledge to select the best options for particular applications. Comparisons between two of the most widely used community ocean models of the terrain-following (sigma or s-coordinate) type, POM and ROMS, demonstrate how numerical algorithms and parameterizations may affect the results and how the same parameterization may affect each model differently. As applications of this type of ocean models often use high resolution grids and additional sophisticated data assimilation schemes in realistic applications, the computational efficiency becomes important, thus emphasis was given here to the computational cost of various configurations and models (Table 1). A new time stepping scheme implemented in ROMS show promising results in allowing the use of time steps larger than that implied by the common CFL stability condition, but on the other

hand the choice of the split between the baroclinic (internal) and the barotropic (external) time steps may require a more careful consideration due to a more elaborate coupling between the two modes. Several new pressure gradient schemes, based on polynomial fits of pressure or density fields, show promising results and compare favorably with more expensive high order schemes. If this well known problem of pressure gradient errors in (atmospheric and oceanic) sigma models is reduced to a manageable level below other numerical errors, it will allow more accurate simulations of a larger range of applications without the need to smooth topographies or the use of very high resolutions. This study could not possibly test all the available options in sigma ocean models. It just demonstrates a few aspects of the models from the point of view of users who would like to know how to chose different parameters, how these choices may affect the results, and the computational cost. Promising approaches for future ocean modeling, not discussed here, are the use of generalized grids that will allow an optimal combination of sigma, z-level and isopycnal grids, such approaches are now being tested by several ocean modeling communities (Mellor et al., 2002; Bleck, 2002).

Acknowledgements

The development of an expert terrain-following ocean modeling system is supported by ONR's Ocean Modeling and Prediction Branch. K. Bryan, G. Mellor, and two reviewers provide useful comments. Computational support for T.E. was provided by the NOAA's Geophysical Fluid Dynamics Laboratory.

References

Arakawa, A., Lamb, V.R., 1977. Computational design of the basic dynamical processes of the UCLA general circulation model. In: Methods in Computational Physics, vol. 17. Academic Press, New York, pp. 174–265.

Asselin, R., 1972. Frequency filters for time integrations. Monthly Weather Review 100, 487–490.

Beckmann, A., Döscher, R., 1997. A method for improved representation of dense water spreading over topography in geopotential-coordinate models. Journal of Physical Oceanography 27, 581–591.

Beckmann, A., Haidvogel, D., 1993. Numerical simulation of flow around a tall isolated seamount. Journal of Physical Oceanography 23, 1736–1753.

Bleck, R., 2002. An oceanic general circulation model framed in hybrid isopycnic-cartesian coordinates. Ocean Modeling 4 (1), 55–88.

Blumberg, A.F., Mellor, G.L., 1983. Diagnostic and prognostic numerical circulation studies of the South Atlantic Bight. Journal of Geophysical Research 88, 4579–4592.

Blumberg, A.F., Mellor, G.L., 1987. A description of a three-dimensional coastal ocean circulation model. In: Heaps, N.S. (Ed.), Three-Dimensional Coastal Ocean Models. Coastal Estuarine Studies, vol. 4. American Geophysical Union, Washington, DC, pp. 1–16.

Canuto, C., Hussaini, M.Y., Quarteroni, A., Zang, T.A., 1988. Spectral Methods in Fluid Mechanics. Springer, Berlin, 567 pp.

Chu, P.C., Fan, C., 1997. Sixth-order difference scheme for sigma coordinate ocean models. Journal of Physical Oceanography 27, 2064–2071.

Chu, P.C., Fan, C., 1998. A three-point combined compact difference scheme. Journal of Computational Physics 140, 370–399.

Courant, R., Friedrichs, K., Lewy, H., 1967. On the partial difference equations of mathematical physics. IBM Journal (March), 215–234.

Ezer, T., 1999. Decadal variabilities of the upper layers of the subtropical North Atlantic: an ocean model study. Journal of Physical Oceanography 29, 3111–3124.

Ezer, T., 2000. On the seasonal mixed-layer simulated by a basin-scale ocean model and the Mellor-Yamada turbulence scheme. Journal of Geophysical Research 105, 16,843–16,855.

Ezer, T., 2001. On the response of the Atlantic Ocean to climatic changes in high latitudes: a sensitivity study with a sigma coordinate ocean model. In: Seidov, D., Maslin, M., Haupt, B. (Eds.), Ocean and Rapid Past and Future Climate Change: North-South Connections. Geophysical Monograph, vol. 126, pp. 199–215.

Ezer, T., Mellor, G.L., 1997. Simulations of the Atlantic Ocean with a free surface sigma coordinate ocean model. Journal of Geophysical Research 102, 15,647–15,657.

Ezer, T., Mellor, G.L., 2000. Sensitivity studies with the North Atlantic sigma coordinate Princeton Ocean Model. Dynamics of Atmospheres and Oceans 32, 155–208.

Gent, P.R., McWilliams, J.C., 1990. Isopycnal mixing in ocean circulation models. Journal of Physical Oceanography 20, 150–155.

Gerdes, R., 1993. A primitive equation ocean circulation model using a general vertical coordinate transformation. 1. Description andtesting of the model. Journal of Geophysical Research 98, 14683–14701.

Greatbatch, R.J., Mellor, G.L., 1999. An overview of coastal ocean models. In: Mooers, C.N.K. (Ed.), Coastal Ocean Prediction. American Geophysical Union, Washington, DC, pp. 31–57.

Griffies, S.M., Boning, C., Bryan, F.O., Chassignet, E.P., Gerdes, R., Hasumi, H., Hirst, A., Treguier, A., Webb, D., 2000. Developments in ocean climate modelling. Ocean Modelling 2, 123–192.

Haney, R.L., 1991. On the pressure gradient force over steep topography in sigma coordinate ocean models. Journal of Physical Oceanography 21, 610–619.

Haidvogel, D.B., Beckmann, A., 1999. Numerical Ocean Circulation Modeling. Imperial College Press, London, 318 pp.

Haidvogel, D.B., Wilkin, J.L., Young, R., 1991. A semi-spectral primitive equation ocean circulation model using vertical sigma and orthogonal curvilinear horizontal coordinates. Journal of Computational Physics 94, 151–185.

Haidvogel, D.B., Arango, H., Hedstrom, K., Beckmann, A., Malanotte-Rizzoli, P., Shchepetkin, A.F., 2000. Model evaluation experiments in the North Atlantic Basin: simulations in nonlinear terrain-following coordinates. Dynamics of Atmospheres and Oceans 32, 239–282.

Hecht, M.W., Wingate, B.A., Kassis, P., 2000. A better, more discriminating test problem for ocean tracer transport. Ocean Modelling 2, 1–15.

Iskandarani, M., Haidvogel, D.B., Boyd, J.P., 1995. A staggered spectral element model with applications to the oceanic shallow water equations. International Journal of Numerical Methods in Fluids 20, 393–414.

Kliem, N., Pietrzak, J.D., 1999. On the pressure gradient error in sigma coordinate ocean models: a comparison with laboratory experiment. Journal of Geophysical Research 104, 29,781–29,799.

Large, W.G., McWilliams, J.C., Doney, S.C., 1994. Oceanic vertical mixing: a review and a model with a nonlocal boundary layer parameterization. Reviews of Geophysics 32, 363–403.

Lin, S.-J., 1997. A finite volume integration method for computing pressure gradient force in general vertical coordinates. Quarterly Journal of the Royal Meteorological Society 123, 1749–1762.

Lin, S.-J., Chao, W.C., Sud, Y.C., Walker, G.K., 1994. A class of the van Leer-type transport schemes and its application to the moisture transport in a general circulation model. Monthly Weather Review 122, 1575–1593.

Lynch, D.R., Gray, W.G., 1980. Finite element simulation of flow in deforming regions. Journal of Computational Physics 36, 135–153.

McCalpin, J.D., 1994. A comparison of second-order and fourth-order pressure gradient algorithms in a sigma coordinate ocean model. International Journal of Numerical Methods in Fluids 18, 361–383.

Mellor, G.L., 1996. User's guide for a three-dimensional, primitive equation, numerical ocean model. Program in Atmospheric and Oceanic Sciences, Princeton University, Princeton, NJ, 40 pp.

Mellor, G.L., 2001. One-dimensional, ocean surface layer modeling, a problem and a solution. Journal of Physical Oceanography 31, 790–809.

Mellor, G.L., Blumberg, A.F., 1985. Modeling vertical and horizontal diffusivities with the sigma coordinate system. Monthly Weather Review 113, 1380–1383.

Mellor, G.L., Ezer, T., 1995. Sea level variations induced by heating and cooling: an evaluation of the Boussinesq approximation in ocean model. Journal of Geophysical Research 100, 20,565–20,577.

Mellor, G.L., Yamada, T., 1982. Development of a turbulent closure model for geophysical fluid problems. Review of Geophysics 20, 851–875.

Mellor, G.L., Ezer, T., Oey, L.-Y., 1994. The pressure gradient conundrum of sigma coordinate ocean models. Journal of Atmospheric and Ocean Technology 11 (Part 2), 1126–1134.

Mellor, G.L., Hakkinen, S., Ezer, T., Patchen, R., 2002. A generalization of a sigma coordinate ocean model and an intercomparison of model vertical grids. In: Pinardi, N., Woods, J.D. (Eds.), Ocean Forecasting: Conceptual Basis and Applications. Springer, Berlin, pp. 55–72.

Mellor, G.L., Oey, L.-Y., Ezer, T., 1998. Sigma coordinate pressure gradient errors and the seamount problem. Journal of Atmospheric and Ocean Technology 15, 1122–1131.

Pacanowski, R.C., Gnanadesikan, A., 1998. Transient response in a *z*-level ocean model that resolves topography with partial cells. Monthly Weather Review 126, 3248–3270.

Pacanowski, R.C., Griffies, S.M., 1999. The MOM 3 Manual. Geophysical Fluid Dynamics Laboratory/NOAA, Princeton, USA, p. 680.

Pietrzak, J., 1998. The use of TVD limiters for forward-in-time upstream-biased advection schemes in ocean modeling. Monthly Weather Review 126, 813–830.

Shchepetkin, A.F., McWilliams, J.C., 1998. Quasi-monotone advection schemes based on explicit locally adaptive dissipation. Monthly Weather Review 126, 1541–1580.

Shchepetkin, A.F., McWilliams, J.C., 2000. The regional ocean modeling system: a split-explicit, free surface, topography-following coordinate ocean model. Geophysics and Planetary Physics, UCLA, Los Angeles, CA, 31 pp.

Shchepetkin, A.F., McWilliams, J.C., 2002. A method for computing horizontal pressure gradient force in an ocean model with non-aligned a vertical coordinate. Journal of Geophysical Research, under revision.

Smagorinsky, J., 1963. General circulation experiments with the primitive equations: I. The basic experiments. Monthly Weather Review 91, 99–164.

Smolarkiewicz, P.K., 1984. A fully multidimensional positive definite advection transport algorithm with small implicit diffusion. Journal of Computational Physics 54, 325–362.

Song, Y.T., 1998. A general pressure gradient formulation for ocean models. Part I: Scheme design and diagnostic analysis.. Monthly Weather Review 126, 3213–3230.

Song, Y.T., Haidvogel, D., 1994. A semi-implicit ocean circulation model using a generalized topography following coordinate system. Journal of Computational Physics 115, 228–248.

Winton, M., Hallberg, R., Gnanadesikan, A., 1998. Simulation of density-driven frictional downslope flow in *z*-coordinate ocean models. Journal of Physical Oceanography 28, 2163–2174.